S1. Stratigraphy

For the present study, new age models have been developed using the same state-of-the-art approach for each of the studied cores. Each age model has been elaborated by combination of two types of control points: (i) radiocarbon (AMS ^{14}C) datings (Manthé, 1998; Dokken and Jansen, 1999; Zumaque et al., 2012; Caulle et al., 2013; Wary et al., 2016) converted to calendar ages using Calib 7.1.0 calibration program (http://calib.qub.ac.uk/calib/) and Marine13 calibration curve (Reimer et al., 2013), with an integrated 405 year marine reservoir correction (Table S2), and (ii) event-based tie-points derived from the correlation of the magnetic susceptibility signals to the NGRIP-GICC05 $\delta^{18}O$ record (North Greenland Ice Core Project members, 2004; Svensson et al., 2008) (i.e. the recommended North Atlantic regional stratotype after Austin and Hibbert, 2012). The rationale is that marine records of magnetic parameters from MIS 3 are consistent across the North Atlantic basin along the path of different overflow branches of the North Atlantic Deep Water and can be tied to the high frequency climatic variability (Dansgaard-Oeschger – DO – cycles) characteristic of this period (Kissel et al., 1999). Chronostratigraphies of the cores have been constructed using this DO event chronostratigraphy after dates from Wolff et al. (2010) (NGRIP-GICC05 derived, see Table S2 and Fig. S1). Core MD95-2010 also benefits from the recovery of ash-layer well-dated horizons (Dokken and Jansen, 1999) (http://doi.pangaea.de/10.1594/PANGAEA.735730; Table S2) used as additional control points. Each age model has been finally established on the basis of a linear interpolation between ages and tie-points.

Stratigraphies of cores MD95-2009 and MD99-2281 are additionally supported by the occurrence of supplementary tie-points (not used but fitting our age model constructions),

independent from climate, derived from the record of the changes in the Earth's magnetic field intensity, namely the two prominent lows attributed to the Mono Lake and the Laschamp excursions (see Kissel et al., 1999; Laj et al., 2004; Zumaque et al., 2012).

S2. Dinocyst counts, transfer function and seasonality signals

Dinocysts were counted in the 10-150 µm fraction after classical palynological preparation of sediment samples (http://www.epoc.u-bordeaux.fr/index.php?lang=fr&page=eq_paleo_pollens). When possible, a minimum of 300 dinocysts were counted in each sample using a Leica Microscope at x400 magnification. Species identification follows (Rochon et al., 1999; Head et al., 2001; Radi et al., 2013). Relative abundances of each species were calculated relative to the total sum of Quaternary dinocysts. Among the dominant species of the four studied cores, one deserves here a special attention – *Islandinium minutum* – as it is strongly related to cold and seasonally sea-ice covered surface environments (Radi et al., 2013). Its highest abundances are observed in areas covered with sea ice between 8 and 12 months/year (Rochon et al., 1999) (Fig. S2). In the Norwegian Sea cores, records of %I.MIN (Fig. S3) clearly indicate lower SST and longer SIC during GI, and milder surface conditions during GS. In the Atlantic core MD99-2281, the %I.MIN signal show low values throughout the studied period, indicative of a strongly reduced SIC duration; the very slight increase of %I.MIN during GS indicate relatively colder sea-surface conditions, thus confirming the difference of pattern observed in-between the Nordic Seas and the North Atlantic Ocean.

Past sea-surface conditions were derived from a transfer function applied to dinocyst assemblages, using the modern analogue technique (see Guiot and de Vernal, 2007, 2011a,

2011b for a review of this technique). Briefly, calculation relies on a statistical comparison of fossil samples to a large set of modern (surface sediment) samples. The five best analogues (i.e. minimal statistical dissimilarity between the species spectra) are selected for the reconstructions. The hydrographic data corresponding to these analogues, compiled from the 2001 version of the World Ocean Atlas for SST and sea-surface salinities (extracted at 10 meters water depth) and from the National Snow and Ice Data Center (NSIDC) of Boulder for sea ice data, are then used to calculate weighted (inversely to the dissimilarity of the analogues) averaged past sea-surface parameters.

Previously, quantitative reconstructions were published for three of the studied cores: cores MD95-2009 and MD95-2010 using a modern dinocyst database including 677 samples (Eynaud et al., 2002), and core MD99-2281 using the 1189 modern sample database (Zumaque et al., 2012).

For the present study, the published dinocyst counts of those cores and the new data of core MD99-2285 were statistically treated with an extended modern database composed of 1207 sites from North Atlantic Ocean, Arctic and sub-Arctic basins, Mediterranean Sea and North Pacific Ocean (database available from the DINO9 workshop, http://pcwww.liv.ac.uk/~dino9/workshops.htm), to provide quantitative reconstructions for hydrological parameters. These include mean summer (July-August-September) and mean winter (January-February-March) SST (respective RMSEP of 1.5 °C and 1.05 °C), mean summer and mean winter SSS (respective RMSEP of 2.4 and 2.3 psu), and mean annual SIC duration (RMSEP of 1.2 month/year). Seasonality signals (Fig. S4) were then determined by subtracting mean winter SST to mean summer SST.

We chose to graphically represent winter SST (Fig. 2) where GI-GS amplitudes are comparable within the four cores, but note that the same patterns are observable in annual

SST records from all the four cores (Fig. S5). These same patterns are also observable in summer SST records from the three Norwegian Sea cores (with even higher amplitudes), but not from the Atlantic core MD99-2281 where an opposite pattern seems to be recorded but with a significantly smaller amplitude as compared to winter SST record. We attribute this behavior to the nodal location of this site, i.e. in the transitional area where (i) during GS, warm Atlantic subsurface waters re-emerge at the surface, and (ii) during GI, the polar front migrates northward/southward during summer/winter (cf. Fig. 3).

S3. Model simulations

Freshwater hosing experiments were conducted using four coupled ocean-atmosphere models (HadCM3, IPSLCM5A, MPI-ESM, EC-Earth) and one ocean-only model (ORCA05; Table S3). Results from the coupled ocean-atmosphere BCM2 model are not considered here, while reported in the original study (Swingedouw et al., 2013). It showed a very different behavior as compared to the five models considered here, and was therefore considered as an outlier in the former ensemble. According to the authors of the original study, this is linked to the fact that the freshwater spread exhibits a different path in BCM2 compared to the five other models, probably in relation with the very low resolution in the ocean in BCM2 (around 3° in the North Atlantic, *cf.* their Fig. 1) compared to the others (from less than 0.5°C to around 1° in the North Atlantic). Nevertheless, considering a multi-model result including BCM2 only slightly changes the pattern of the response and its amplitude.

Note that results from the ocean-only model (ORCA05) display strong similarities with the ones from the four coupled ocean-atmosphere models. It implies that the structure of the

simulated changes is mostly driven by oceanic processes and weakly due to atmospheric feedbacks.

S4. SST, SIC and SSS anomalies

Mean annual SST, SIC duration, and SSS anomalies were calculated for each core (respectively Table 1, Table 2, and Table S4) as follows: mean winter and mean summer SST and SSS, as well mean annual SIC duration, were determined over (i) the stadial period, comprising GS 10, 9, 8, 7 and 6, and (ii) the interstadial period, comprising GI 10, 9, 8, 7, 6, and 5, using the GICC05 age limits of each GS/GI from Wolff et al. (2010). Then, mean annual SST (and SSS), for GS and for GI periods, were determined by averaging mean winter and mean summer SST (SSS). Finally, mean annual SST (SSS and SIC) anomalies were obtained by subtracting mean annual GI SST (SSS and SIC) to mean annual GS SST (SSS and SIC; i.e. GS minus GI).

S5. Relative percentages of *Neogloboquadrina pachyderma* sinistral coiling (%NPS)

Planktonic foraminifera were counted in the > 150 µm fraction after classical preparation of sediment samples (washed through a 150 µm sieve before being dried). When possible, a minimum of 300 specimens were counted in each sample, and relative abundances of each species were determined (Eynaud et al., 2002; Zumaque et al., 2012; Wary, 2015), revealing nearly continuous monospecific dominance of NPS (except in core MD99-2281), a taxon usually used to track the migration of cold polar waters (Eynaud et al., 2009).

S6. Dinoflagellates versus NPS depth habitats

Noticeable differences exist in the depth habitats of dinoflagellates and NPS, which, if not taken into account, can lead to inaccurate interpretations. Dinoflagellates are known to be mainly restricted to the uppermost 50 meters of the water column (Sarjeant et al., 1974), with autotrophic organisms restricted to the photic layer and heterotrophic organisms feeding on autotrophic organisms. This implies that dinocysts are tracers of sea-surface *stricto sensu* conditions. On the contrary, growing evidence of the mesopelagic affinity characterizing the planktonic foraminifera NPS has emerged during the last decades (Carstens and Wefer, 1992; Bauch et al., 1997; Carstens et al., 1997; Hillaire-Marcel and Bilodeau, 2000; Volkmann and Mensch, 2001; Simstich et al., 2003; Hillaire-Marcel et al., 2004; Kretschmer et al., 2016). This involves that dinocysts and NPS may not track the same water mass, i.e. that NPS may not track sea-surface conditions as often admitted but rather subsurface or near-surface conditions. The present study illustrates well this possibility of decoupling, with (i) in the case of a strong stratification of the upper few hundred meters of the water column (GS), dinocyst and NPS displaying opposite signals, i.e. tracking different water masses (the surface and subsurface, respectively), and (ii) in the case of reduced/zero stratification, dinocyst and NPS displaying concordant signals, i.e. tracking the same homogeneous upper water mass.

Figure S1. Information regarding the age model construction of the studied cores. (a) Age versus depth plots of the respective chronological constrains used to built the chronology (Table S2). (b) Alignment of magnetic susceptibility (MS) records of the respective studied cores to NGRIP GICC05 $\delta^{18}O$ record (North Greenland Ice Core Project members, 2004; Svensson et al., 2008). Vertical lines illustrate the position of the tie-points derived from peak matching.

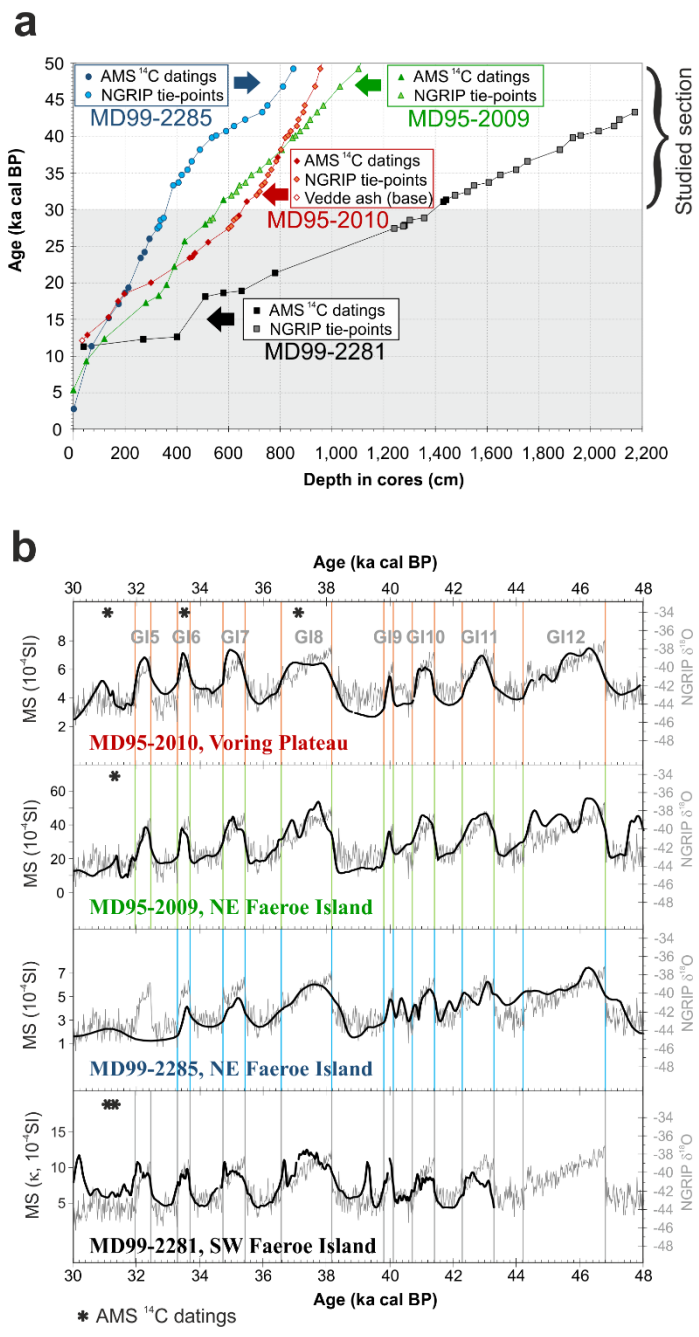

Figure S2. *Islandinium minutum* distribution and ecology. (a) *Islandinium minutum* distribution within the modern dinocyst database made of 1207 points. (b) Oceanic temperatures at 10 mbsl (WOA09 data; Locarnini et al., 2010). (c) Sea-ice cover (with concentration greater than 50%) duration within the modern dinocyst database made of 1207 points (after data provided by the National Climate Data Centre in Boulder). These maps demonstrate the strong link of this dinocyst taxon with cold and seasonally sea-ice covered surface environments.

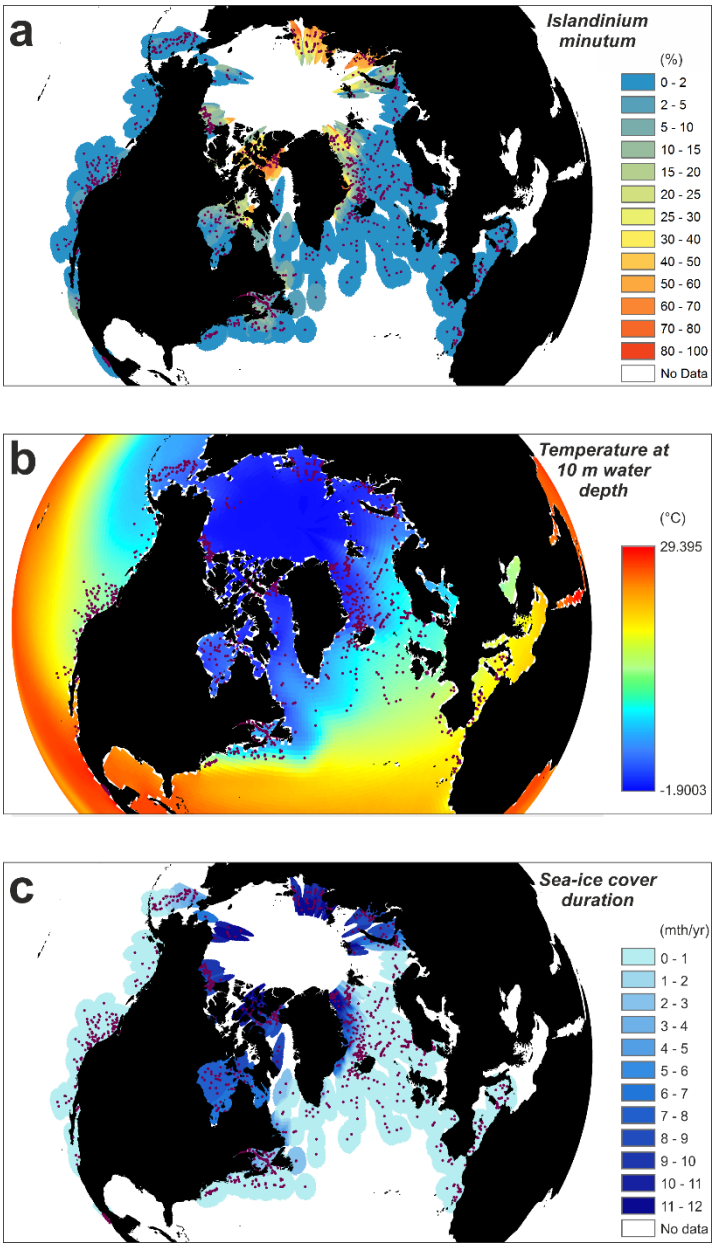

Figure S3. Relative percentage of *Islandinium minutum* within the four studied cores. For each core (from a to d) the %I.MIN records, indicative of colder SST and longer SIC, are compared to the magnetic susceptibility signals which can be directly aligned with Greenland climate variability as detected within (e) NGRIP $\delta^{18}O$ record (North Greenland Ice Core Project members, 2004; Svensson et al., 2008). Gray bands highlight low NGRIP $\delta^{18}O$ and low MS values, i.e. stadial periods. It is worth noting the opposite scheme described by %I.MIN variations within the Nordic Seas *versus* in the Atlantic sector, which again illustrates the seesaw pattern observed between Nordic Seas and North Atlantic.

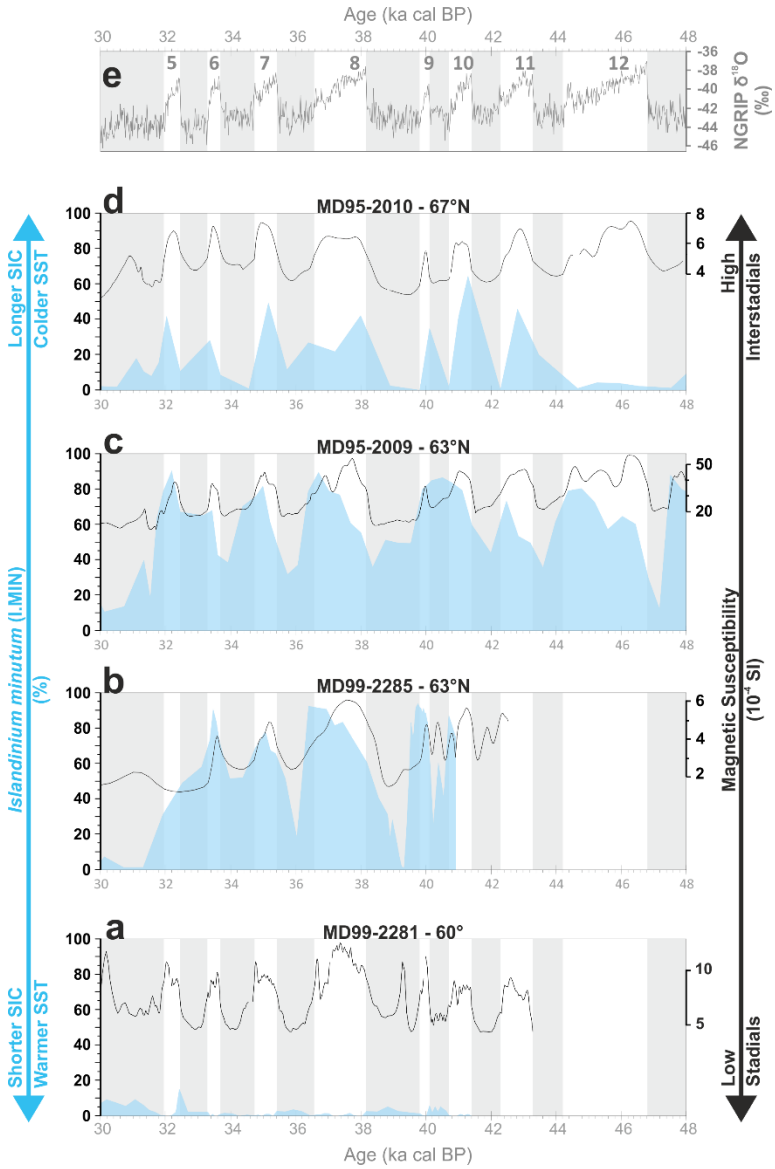

Figure S4. Sea-surface seasonality contrasts, calculated in the different cores as summer SST minus winter SST and plotted along with the reference NGRIP $\delta^{18}O$ stratotype (GICC05 age scale; North Greenland Ice Core Project members, 2004; Svensson et al., 2008). Sea-surface seasonality values are shaded relatively to the mean value obtained over the studied period within each core (threshold value indicated in gray next to each record). Triangles indicate modern values of summer SST (red), winter SST (blue), and seasonality (black) for each study site (WOA09 data; Locarnini et al., 2010). As in Fig. S3, gray bands highlight low NGRIP $\delta^{18}O$ and low MS values, i.e. stadial periods.

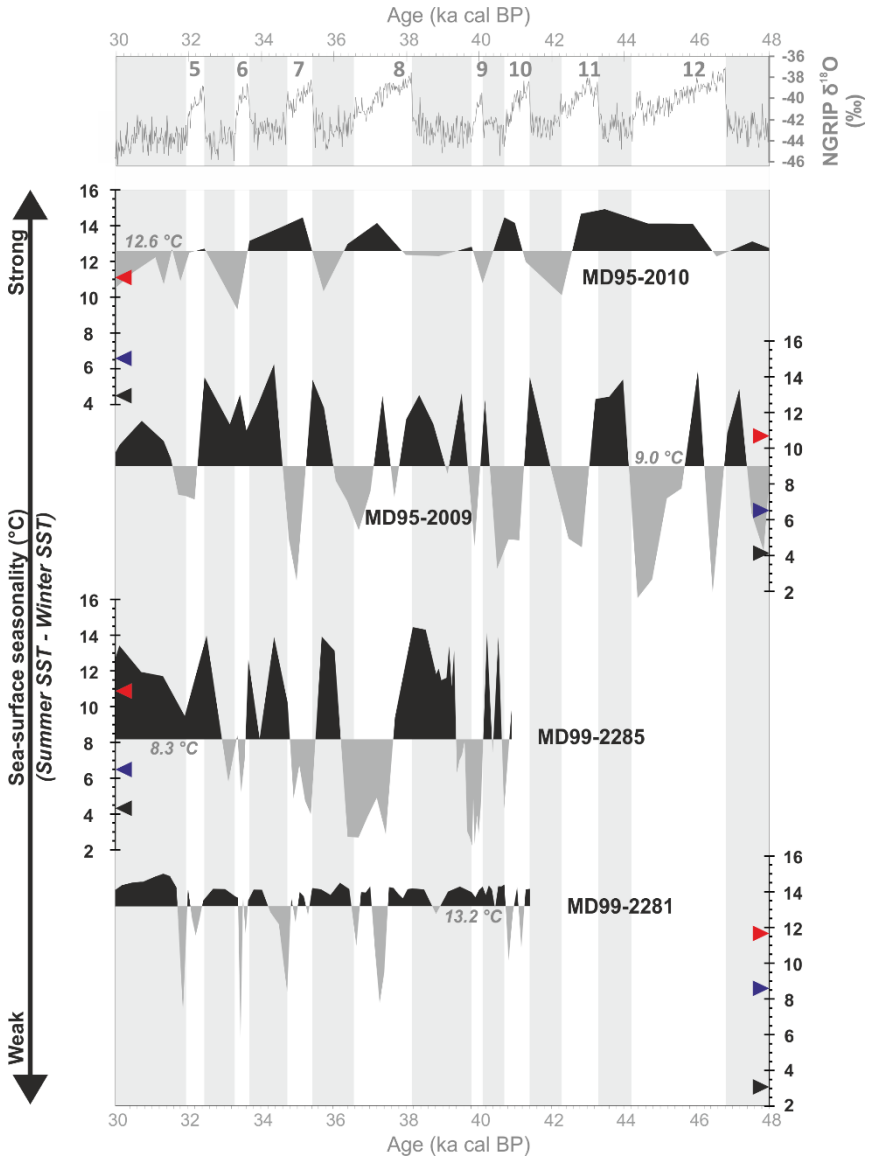

Figure S5. Annual and seasonal SST records in the four studied cores plotted along with NGRIP $\delta^{18}O$ record (GICC05 age scale; North Greenland Ice Core Project members, 2004; Svensson et al., 2008).

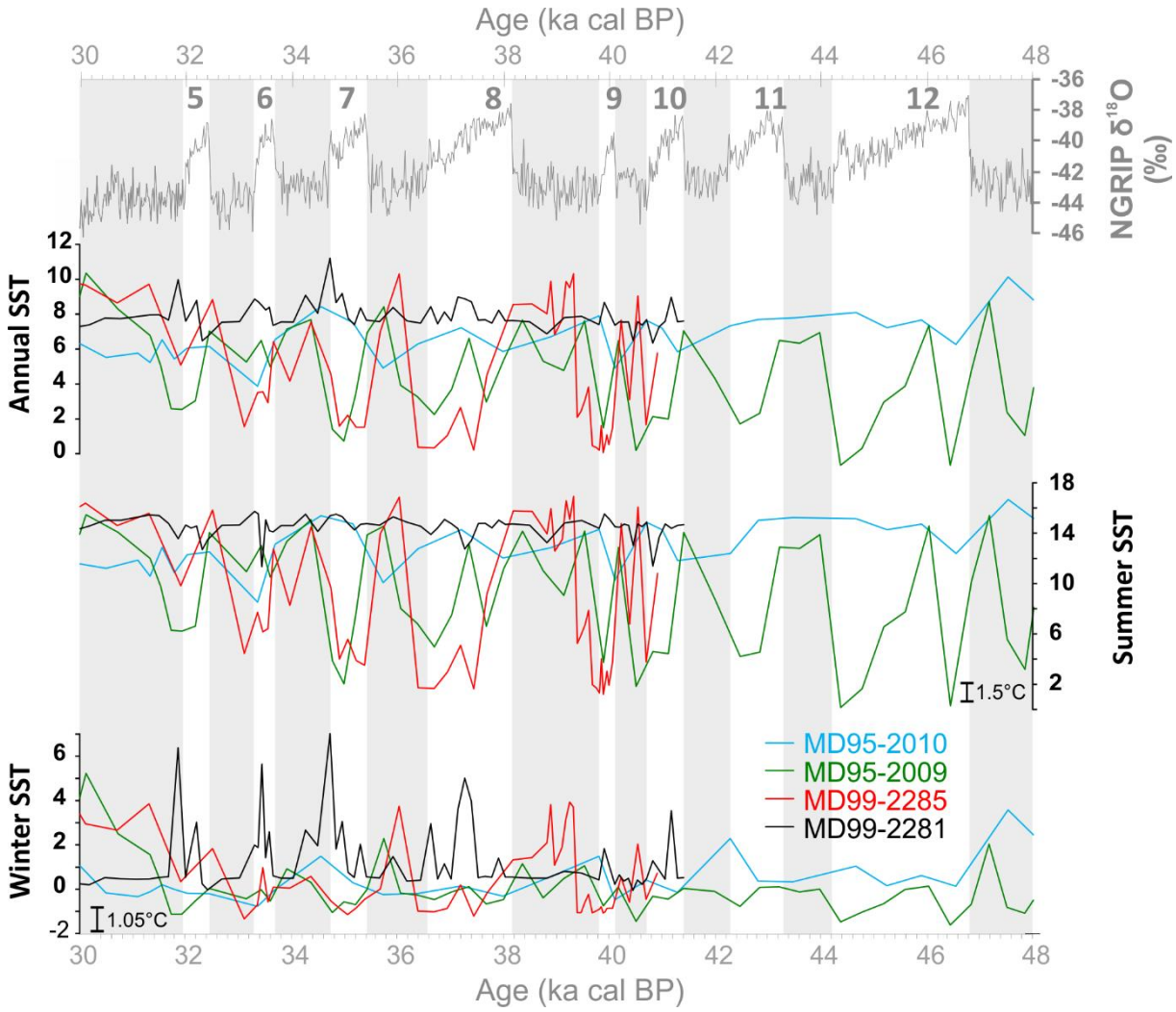

Figure S6. Five-member ensemble mean of barotropic stream function anomalies. Colors represent anomalies between hosing and control experiments averaged over the 4th decade. In contours is the control simulation barotropic stream function averaged over the historical era.

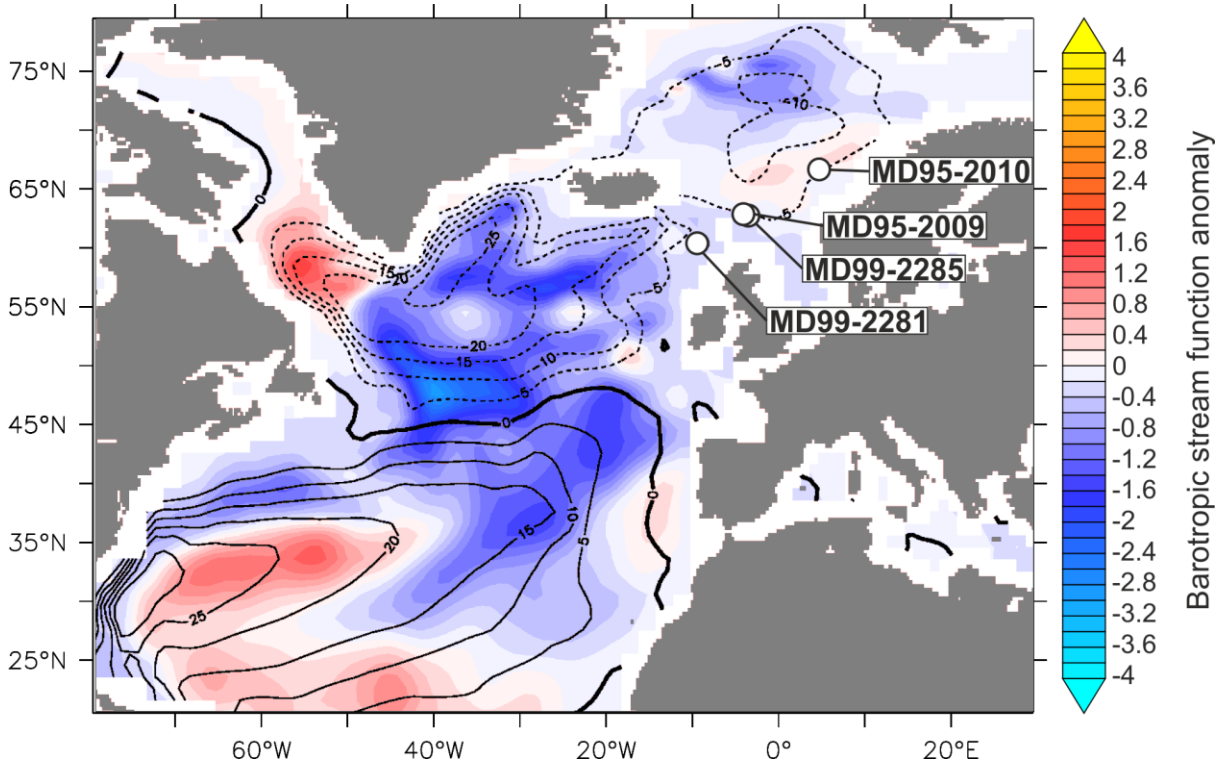

Table S1. Location of studied marine cores.

Core	Latitude (°N)	Longitude (°E)	depth (mbsl)
MD95-2010	66.68	4.57	1,226
MD95-2009	62.74	-4.00	1,027
MD99-2285	62.69	-3.57	885
MD99-2281	60.34	-9.46	1,197

* mbsl: meters below sea level.

Table S2. Age constrains for each of the studied cores.

Table S3. Characteristics of the five models considered.

Model	Institute	Type*	Ocean	Atmosphere	Reference
HadCM3	Hadley Centre	OAGCM	No name 1.25 x 1.25, L20	HadAM3 91 x 76, L19	(Gordon et al., 2000)
IPSLCM5A	Institut Pierre Simon Laplace	OAGCM	NEMO 2°, L31	LMD5 96 x 96, L39	(Dufresne et al. 2013)
MPI-ESM	MPI	OAGCM (ESM)	MPI-OM 1.5°, L40	ECHAM6 T63-L47	(Jungclaus et al., 2013)
ORCA05	GEOMAR	OGCM	NEMO 0.5°, L46	CORE.v2 Forcing	(Biastoch et al., 2008)
EC-Earth	DMI	OAGCM	NEMO 1°, L42	IFS T159-L31	(Sterl et al., 2012)

* OAGCM: Ocean-Atmosphere General Circulation Model; OGCM: Ocean General Circulation Model; ESM: Earth System Model

Table S4. SSS anomalies.

Core	Number of samples		GS SSS (psu)			GI SSS (psu)			Mean annual SSS anomalies (GS-GI; psu)
	GS	GI	mean winter	mean summer	mean annual	mean winter	mean summer	mean annual	
MD99-2281	23	39	32.1	31.3	31.7	32.4	31.6	32.0	-0.3
MD99-2285	26	22	32.7	31.6	32.2	32.9	31.0	32.0	0.2
MD95-2009	12	17	32.0	30.9	31.5	32.0	31.0	31.5	0.0
MD95-2010	6	9	32.0	31.1	31.5	31.8	30.4	31.1	0.4